

Article

Design and Experiment of an Underactuated Broccoli-Picking Manipulator

Huimin Xu ¹ , Gaohong Yu ^{1,2,*}, Chenyu Niu ^{1,3}, Xiong Zhao ^{1,2}, Yimiao Wang ¹ and Yijin Chen ¹

¹ College of Mechanical Engineering, Zhejiang Sci-Tech University, Hangzhou 310018, China; 202010601017@mails.zstu.edu.cn (H.X.); zhaoxiong@zstu.edu.cn (X.Z.)

² Key Laboratory of Transplanting Equipment and Technology of Zhejiang Province, Hangzhou 310018, China

³ New H3C Artificial Intelligence Technologies Co., Ltd., Hangzhou 310018, China

* Correspondence: yugh@zstu.edu.cn

Abstract: Mature broccoli has large flower balls and thick stems. Therefore, manual broccoli picking is laborious and energy-consuming. However, the big spheroid vegetable-picking manipulator has a complex structure and poor enveloping effect and easily causes mechanical damage. Therefore, a broccoli flower ball-picking manipulator with a compact structure and simple control system was designed. The manipulator was smart in structure and stable in configuration when enveloped in flower balls. First, a physical damage test was carried out on broccoli according to the underactuated manipulator's design scheme. The maximum surface pressure of the flower ball was 30 N, and the maximum cutting force of the stem was 35 N. Then, kinematic analysis was completed, and the statical model of the underactuated mechanism was established. The dimension of the underactuated mechanism for each connecting rod was determined based on the damage test results and design requirements. The sizes of each connecting rod were 50 cm, 90 cm, 50 cm, 90 cm, 50 cm, 60 cm, and 65 cm. The statical model calculated the required thrust of the underactuated mechanism as 598.66–702.88 N. Then, the manipulator was simulated to verify its reliability of the manipulator. Finally, the manipulator's motion track, speed, and motor speed were determined in advance in the laboratory environment. One-hundred picking tests were carried out on mature broccoli with a 135–185 mm diameter. Results showed that the manipulator had an 84% success rate in picking and a 100% lossless rate. The fastest single harvest time in the test stand was 11.37 s when the speed of the robot arm was 3.4 m/s, and the speed of the stepper motor was 60 r/min.

Keywords: broccoli-picking; underactuated mechanism; manipulator; simulation; test



Citation: Xu, H.; Yu, G.; Niu, C.; Zhao, X.; Wang, Y.; Chen, Y. Design and Experiment of an Underactuated Broccoli-Picking Manipulator.

Agriculture **2023**, *13*, 848. <https://doi.org/10.3390/agriculture13040848>

Academic Editors: Cheng Shen, Zhong Tang and Maohua Xiao

Received: 25 March 2023

Revised: 6 April 2023

Accepted: 6 April 2023

Published: 11 April 2023



Copyright: © 2023 by the authors. Licensee MDPI, Basel, Switzerland. This article is an open access article distributed under the terms and conditions of the Creative Commons Attribution (CC BY) license (<https://creativecommons.org/licenses/by/4.0/>).

1. Introduction

China is a major producer of vegetables in the world, with its production scale and export scale ranking first in the world [1]. As a vegetable favored by the world, broccoli's planting scale is increasing yearly. At present, the total planting area in China is about 100,000 hectares, and the output accounts for 50% of the global total [2,3]. With the increase in planting scale, traditional manual harvesting is time-consuming and laborious; therefore, the development of picking equipment is urgently needed [3,4].

The design of a manipulator in vegetable-picking equipment is very important and requires a stable structure, accurate picking, fast response, and minimal damage to the crop [5,6]. Developed countries began to study picking robots in the 1960s, and the research and development of vibrating, suction, shear, and other manipulators promoted the mechanization of picking equipment, but the actual efficiency was not high [7–9]. At present, fruit and vegetable picking is accomplished by designing a manipulator with a stable structure and coordinating with vision [10–12]. Kinugawa et al. [13] designed an underactuated manipulator for circular plates, which is not applicable to plates with other shapes. Xiong et al. [14] improved the flexibility of the end-effector for the difficult task

of picking in an unstructured environment and carried on a two-arm cooperative robot to complete strawberry picking. However, due to the lack of flexibility of the end-effector, the success rate of picking was 70%. Arad et al. [15] developed a sweet pepper-picking robot with six degrees of freedom, but its picking efficiency could not be guaranteed owing to poor algorithm recognition. Although the research and development of picking equipment started late in China, it is developing rapidly now. Various kinds of picking equipment, such as pneumatic apple picking, hand-held tea tender shoot picking, cooperative kiwi picking, and under-driven grape picking, have emerged one after another [16–19]. The underactuated manipulator has good grasping stability, a strong envelope, and high flexibility [20–22]. Yang et al. [20] proposed a new underactuated manipulator, which has three degrees of freedom and ensures the stability of grasping but is not applicable to crops. The humanoid finger mechanism designed by Yin et al. [19] ensures flexible grasping by installing torsional springs with different stiffness coefficients at the knuckle limit, but the structural strength of the mechanism cannot be determined. Ma et al. [23] designed a Y-type underactuated manipulator according to the growth characteristics of sweet pear. Although the picking rate of the device is high, the degree of damage caused by the picking of this manipulator cannot be judged.

Broccoli flower balls are big, have an unequal diameter, and have a thick stem. Therefore, few robot hands are suitable for enveloping flower balls. At present, the mechanized harvesting equipment of cabbage uses high-horsepower tractors loaded with harvesters to complete one-time harvesting. Although highly efficient, it has no selective harvesting function [24]. Blok [25] et al. developed a broccoli image recognition system to solve the problem of selective harvesting. Although selective harvesting can be achieved, the harvesting efficiency is too low. Lapalmeagtech Co., Ltd. combined Sami4.0 [26] with a broccoli harvester to develop a fully automatic harvesting robot. Although the harvester is highly efficient, its large fuselage is not suitable for use in hilly areas. In China, Shandong Hualong Agricultural Equipment Co., Ltd. (Qingzhou, China) developed a broccoli-harvesting and loading machine, which relies on human labor to harvest broccoli and place the flower balls into the harvesting conveyor belt, but a whole mechanized harvesting operation has not been realized [27]. Yu et al. [28] designed a hanging bucket for broccoli harvesting, which can reduce the labor force. However, the actual nature of the device is similar to that of Shandong Hualong's broccoli-harvesting device, which relies on human resources. However, the broccoli-harvesting equipment of China Agricultural University [29] and Jiangsu University [30] is still in the research and development stage.

In this paper, an underactuated broccoli-picking manipulator was designed to solve problems in the manual picking of mature broccoli, such as big flower balls, thick stems, and huge time and labor consumption. The underactuated broccoli-picking manipulator will be designed to have a compact underactuated structure and a simple control system to realize the stable picking of flower balls. First, physical damage tests were carried out to determine the range of flower ball surface pressure and stem-cutting force. Then, the mechanical structure and control system of the manipulator was designed from the view of the statics of the picking mechanism. Finally, a picking test bed was set up to carry out the indoor picking test.

2. Design Scheme and Working Principle of the Underactuated Broccoli-Picking Manipulator

In this paper, 300 mature Zhejiang 'Tai Lu' series were selected for studying broccoli's biological character data statistics. The physical characteristics of suitable broccoli were analyzed, as shown in Figure 1. The suitable characteristics were a flower ball diameter Φ of 14–18 cm, a plant height h_1 of 45–50 cm, a stem diameter Φ_1 of 0.34–0.46 cm, a flower ball height h of 7–9 cm, and a harvested plant height h_3 of 12–15 cm.

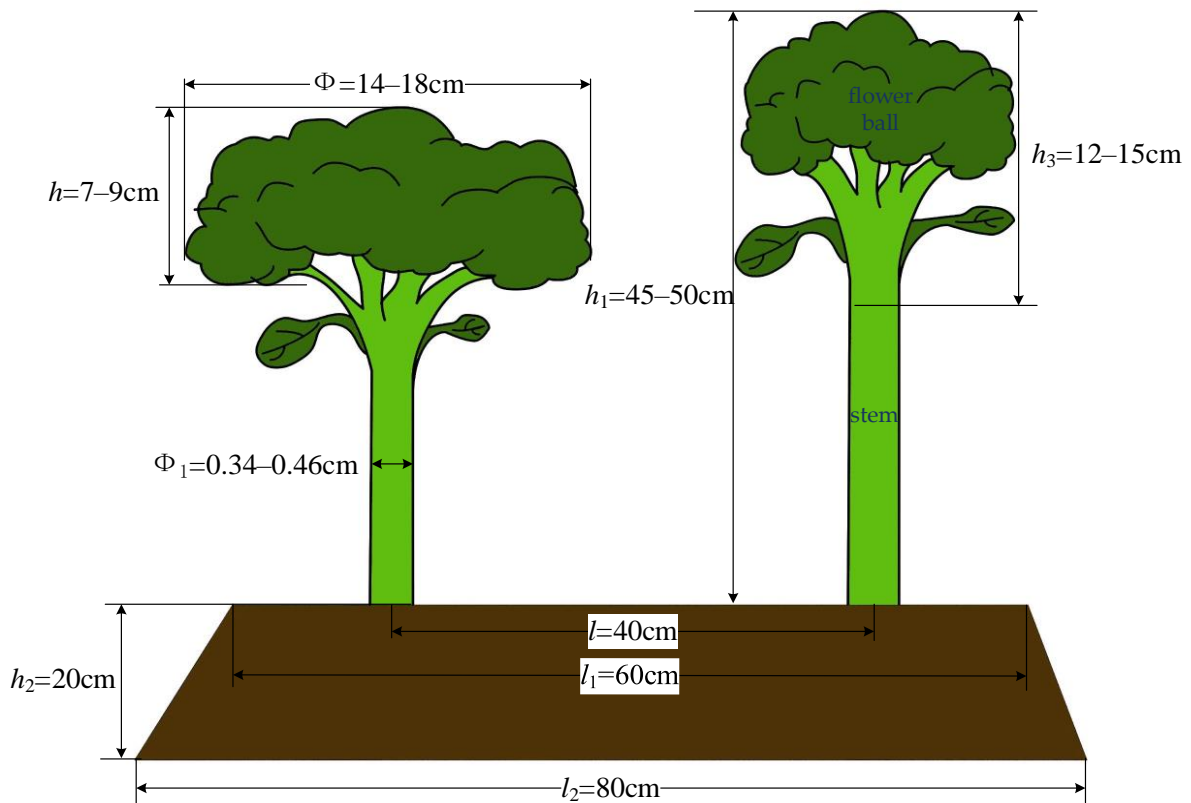


Figure 1. Planting patterns and biological characteristics of broccoli.

A single-stepper motor driven by an underdrive manipulator with two degrees of freedom, which was designed based on a compact underdrive structure, fewer drive actuators, a simple and efficient motion control system, broccoli physical characteristics, and low-loss picking agricultural requirements, can achieve the low-loss enveloping of flower balls with different diameters. The structure of the manipulator is shown in Figure 2.

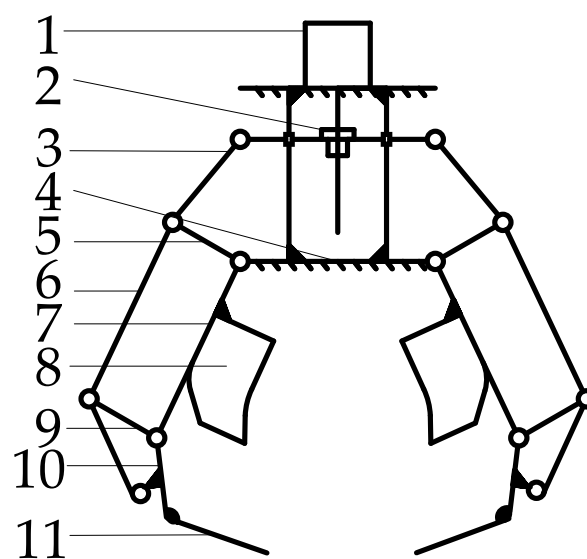


Figure 2. Schematic diagram of manipulator structure: 1 stepper motor; 2 lift platforms composed of worm-and-nut; 3 drive-rod; 4 frame bottom plates; 5, 6 linkage; 7, 9 rockers; 8 clamp guard plates; 10 swing-rod; 11 cutting-blade.

The manipulator is composed of a set of symmetrical underactuated clamping mechanisms, clamping guard plates, cutting blades, and a single-stepper motor, which is picked by a clamping–cutting method. The working principle is shown in Figure 3. The manipulator moves directly above the broccoli and enters the picking area (Figure 3a). Under the action of drive rod force, the clamp guard plates (8) envelope the flower ball (Figure 3b) while the rocker (7) remains motionless. At this time, the rocker (9) drives the swing-rod (10) on the cutting blade (11) to allow the closure of the cutting blades and complete the stem cutting (Figure 3c). Finally, the manipulator driven by the motor picks the flower ball (Figure 3d).

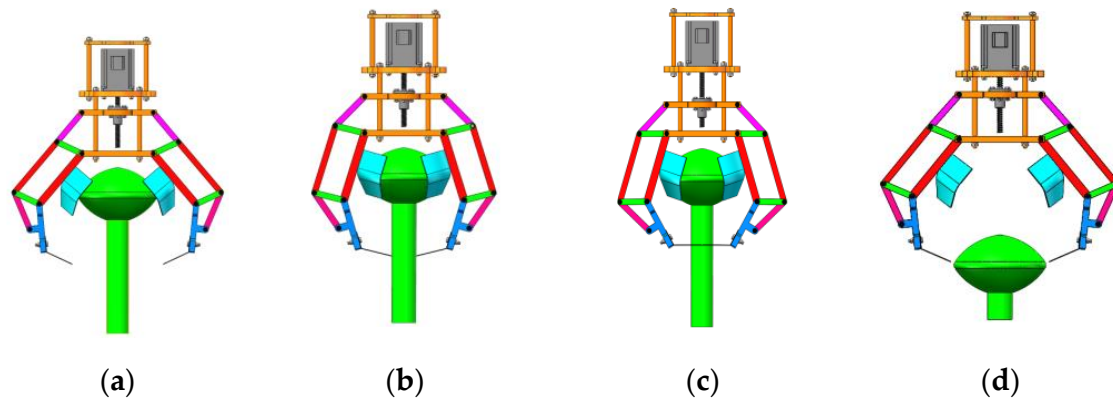


Figure 3. Working principle diagram of picking manipulator: (a) The manipulator enters the area to be picked, (b) Envelope flower ball, (c) Clamp–cut flower ball, and (d) Release flower ball.

3. Mechanism Design of the Underactuated Manipulator

3.1. Determination of the Range of Flower Ball Surface Pressure and Stem-Cutting Force

Broccoli picking involves two actions: enveloping and cutting. The enveloping action is performed by the clamping pressure of the underactuated mechanism, and stem separation is performed by the cutting tool. The maximum clamping pressure on the flower ball surface and the cutting force of the stem needs to be determined to provide a theoretical basis for the design of the rod length of the mechanical hand. The clamping action of the manipulator is composed of four contact forces: clamping pressure $F_1 = F_1'$ and cutting force $F_3 = F_3'$ (Figure 4).

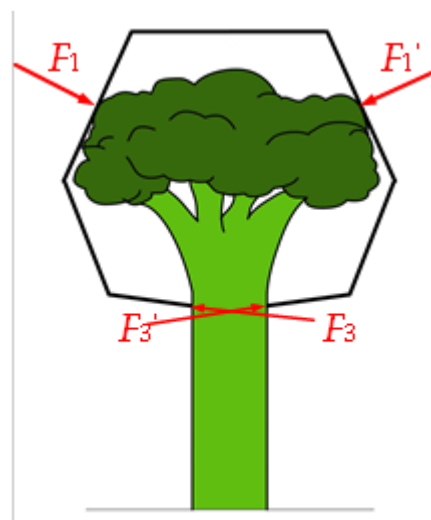


Figure 4. Clamping workspace of the manipulator.

An LDW-1 universal material test machine and cutting tool (304 stainless steel; length, 80 mm; width, 50 mm; thickness, 2 mm; tool point angle, 8°) was used. Thirty flowers with no surface damage were selected to determine the flower surface pressure and stem-cutting force, as shown in Figure 5.

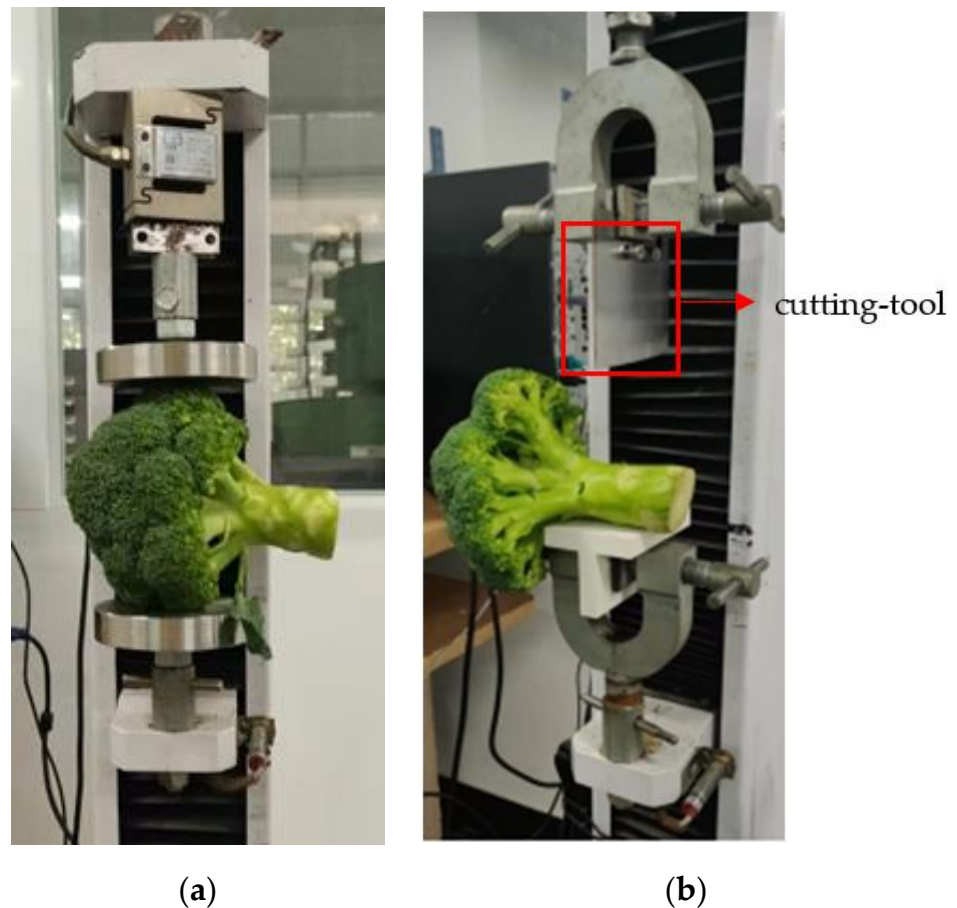


Figure 5. Broccoli physical damage test: (a) Flower ball pressure test; (b) Stem-cutting force test.

The dynamic compression mold of the universal material test machine was operated at a uniform speed of 10 mm/min. Different loads (30, 40, and 50 N) were applied to the surface of the flower ball, and the damage degree was compared and analyzed, as shown in Figure 6.

When the pressure was 30 N, the surface of the flower ball had no obvious damage. When the pressure was 40 N, small flower buds on the compressed surface of the flower ball were slightly deformed, and the small flower buds on the compressed part were damaged. When the pressure was 50 N, the small stem on the inner surface of the flower ball under pressure was deformed, and the small bud under pressure was damaged seriously. Therefore, the clamping pressure was maintained at 25–30 N, which can ensure the non-destructive enveloping of the flower ball.

The fixture of the moving platform on the test machine drove the cutting tool to move at uniform speeds of 30, 80, and 100 mm/min, and 30 groups of cutting tests were carried out. When the cutting blade was in contact with the broccoli stem, the force sensor on the test machine could detect the cutting force in real-time. The cutting force statistics are shown in Figure 7. Each dot in Figure 7 represents the maximum stem-cutting force for each set of tests. In the 30 groups of stem-cutting force, the cutting force represented by red dots was less than that of blue dots and more than that of green dots. The blue dot is the maximum cutting force of 37.28 N, the green dot is the minimum cutting force of 28.36 N, and the average cutting force is 34.89 N. According to the above cutting force

characteristics, keeping the cutting force at 30 N–35 N can ensure that the stems can be cut and separated.

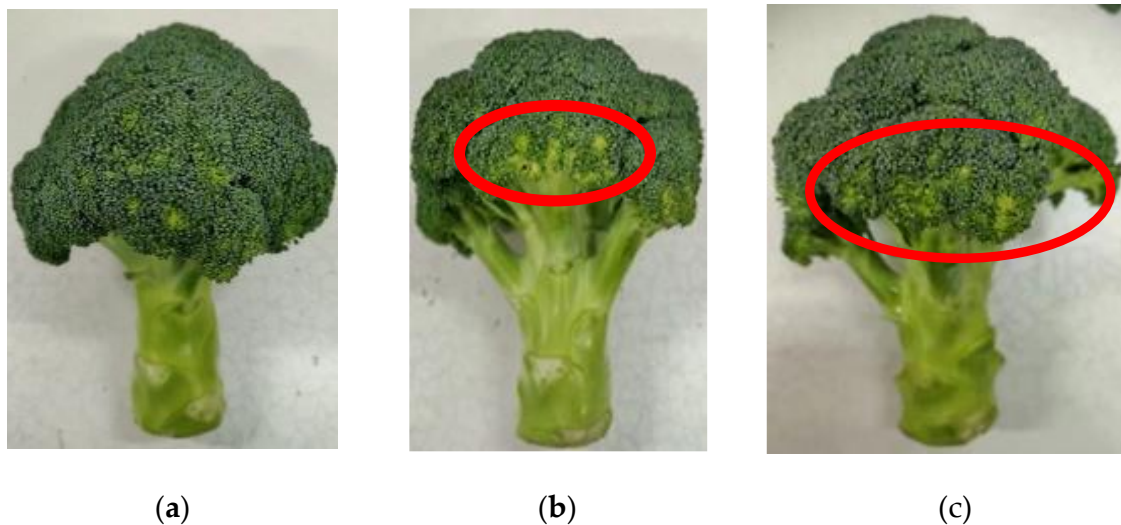


Figure 6. Comparison of pressure damages on broccoli surfaces at different pressures: (a) 30 N; (b) 40 N; (c) 50 N.

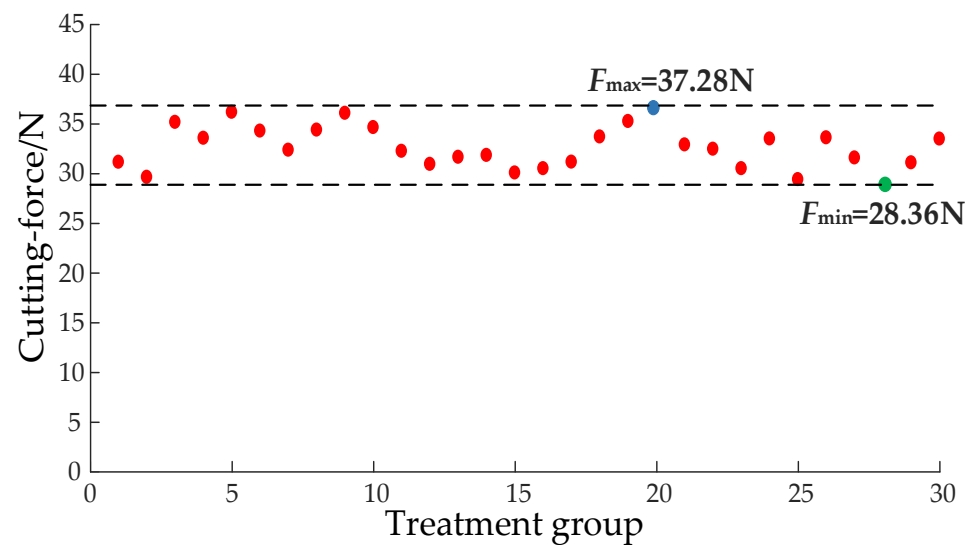


Figure 7. Stem-cutting force test statistics.

3.2. Kinematics Analysis of the Underactuated Mechanism

As shown in Figure 8, the underdrive mechanism designed in this paper is bilaterally symmetric. Therefore, one side of the mechanism was analyzed. When the underactuated mechanism was not in contact with the target object, the relative position of each linkage in the mechanism remained unchanged under the constraint of the torsional spring. The meaning of specific mathematical symbols can be found in Table 1. The specific meanings of mathematical symbols in Figure 8 can be referred to in Table 1. The red characters θ_1 , θ_2 , and θ_3 in Figure 8 respectively represent angle variations of rods AB , AD , and DK .

The four-bar mechanism has the following form:

$$\begin{cases} \begin{bmatrix} \dot{\theta}_2 \\ \dot{\theta}_3 \end{bmatrix} = \begin{bmatrix} 1 & -A \\ 0 & 1 \end{bmatrix} \begin{bmatrix} \dot{\theta}_1 \\ \dot{\theta}_3 \end{bmatrix} \\ J_w = \begin{bmatrix} 1 & -A \\ 0 & 1 \end{bmatrix} \end{cases}, \tag{2}$$

where A is shown in the following equations:

$$\begin{cases} A = \frac{(\sqrt{1-B} + \sin \varphi_2)\sqrt{1-C}}{\sqrt{1-B}(\sqrt{1-C} + \sin \varphi_1)} = 1 \\ B = \frac{[a^2 + b^2 - c^2 + 2cd \cos \varphi_2 - d^2]^2}{4a^2b^2} = \cos^2 \varphi_2 \\ C = \frac{[c^2 + b^2 - a^2 + 2ad \cos \varphi_1 - d^2]^2}{4b^2c^2} = \cos^2 \varphi_1 \end{cases}, \tag{3}$$

Therefore, when the slider E moves down to drive the drive rod BG to move, the underdrive mechanism rotates around base point A . When the clamping guard plates contact the surface of the flower ball, the rocker AD stops moving. The driving force drives the swing rod DK to move and closes the cutting blade to overcome the binding force of the torsional spring and complete the clamping action.

3.3. Statics Analysis of the Underactuated Mechanism

As shown in Figure 9, the unilateral clamping mechanism drives rod BG to move through spiral rotation and drives the four-bar mechanism to complete the whole moving process. The specific meanings of mathematical symbols in Figure 9 can be referred to in Table 1. The red characters F_1 , F_2 , and F_3 in Figure 9 respectively represent the pressure on the surface of the flower ball, the force on the DK rod, and the cutting force of the stem.

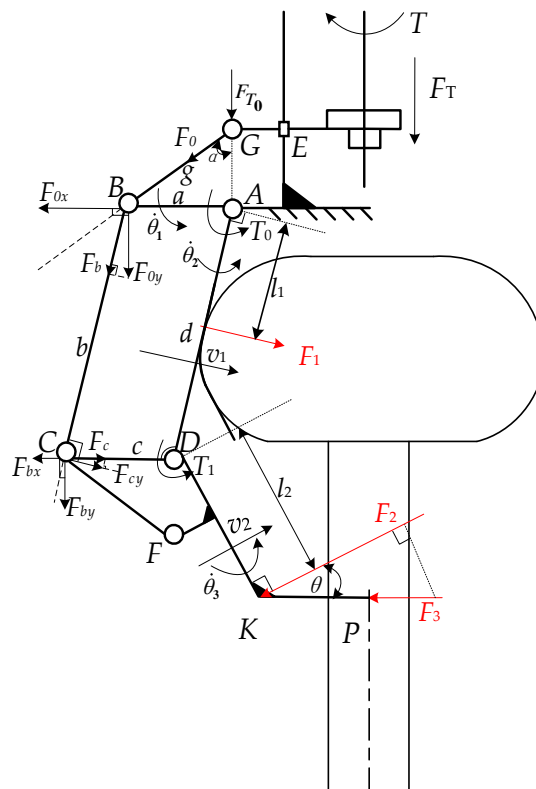


Figure 9. Statics analysis diagram of underactuated mechanism.

In Figure 9, rod GE is pushed down by the left thrust F_{T0} to rotate the driving rod GB , making the four-bar mechanism rotate around base point A . The total thrust F_T and the force of rod BG are shown in Equations (4) and (5):

$$F_T = 2F_{T0}, \tag{4}$$

$$F_0 = F_{T0} \cos \alpha, \tag{5}$$

The force F_b of rod BC is the component force F_{0y} of rod BG as shown in Equation (6):

$$\begin{cases} F_{0y} = F_0 \sin(\frac{\pi}{2} - \alpha) \\ F_b = F_{0y} \sin \varphi_1 \end{cases}, \tag{6}$$

The underactuated mechanism approaches the flower ball under the force F_{cy} perpendicular to the rod BC as shown in Equation (7):

$$\begin{cases} F_c = F_{bx} \\ F_{bx} = F_b \sin \varphi_1 \\ F_{cy} = F_c \sin \varphi_1 \end{cases}. \tag{7}$$

Therefore, the torque T_0 applied by linkage AB around point A is shown in Equation (8):

$$T_0 = aF_{T0} \cos \alpha \sin(\frac{\pi}{2} - \alpha) \cos(\alpha + \theta_1) = aF_{0y} \cos(\alpha + \theta_1), \tag{8}$$

When picking is completed, rod AD and cutting blade KP are constrained by F_1 and F_3 . The mechanical model of the unilateral underdrive is [19,20]:

$$\mathbf{T}^T \boldsymbol{\omega} = \mathbf{F}^T \mathbf{v}, \tag{9}$$

Each vector in Equation (9) can be obtained according to Figure 9.

$$\begin{cases} \mathbf{T}^T = [T_0 \quad T_1]^T \\ \boldsymbol{\omega}^T = [\dot{\theta}_1 \quad \dot{\theta}_3]^T \\ \mathbf{F}^T = [F_1 \quad F_2]^T \\ \mathbf{v}^T = [v_1 \quad v_2]^T \end{cases}, \tag{10}$$

In Equation (10), the torsional spring torque is $T_1 = -(k\theta_3 + T_0^1)$, k is the stiffness coefficient of the torsional spring ($k = 52.85 \text{ N}\cdot\text{mm}/^\circ$), and T_0^1 is the initial torque of the torsional spring ($T_0^1 = 317.1 \text{ N}\cdot\text{mm}$).

According to the relation between the contact force and input torque, the contact force vector of the underdriven mechanism can be obtained using the virtual work principle as follows:

$$\mathbf{F} = \mathbf{TJ}_v^{-T} \mathbf{J}_w^{-T}, \tag{11}$$

Clamping pressure F_1 and cutting force F_3 can be obtained from Equation (11).

$$\begin{cases} F_1 = -\frac{(1 - Al_1 \cos \theta_3)T_0 + (d \cos \theta_3 + l_2)T_1}{l_1 l_2} \\ F_2 = \frac{AT_0(d \cos \theta_3 - l_2) + (l_1 \cos \theta_3 + l_2)T_1}{l_1 l_2} \\ F_3 = \frac{AT_0(d \cos \theta_3 - l_2) + (l_1 \cos \theta_3 + l_2)T_1}{l_1 l_2 \cos \theta} \end{cases}, \tag{12}$$

According to Equation (12), the clamping pressure F_1 and cutting force F_3 are related to T_0 and T_1 , whereas $\theta_1, \theta_2, \theta_3$, and other angles affect the motion position of the mechanism, as shown in Figure 8. The related parameters are listed in Table 1.

3.4. Parameter Determination of Each Rod of the Underactuated Mechanism

In this paper, a stepper motor, model 57HD5401-110, with a torque of 1.2 N·m, was selected as the driving actuator of the manipulator, together with the 4 mm lead of a TBI high-precision linear screw. The thrust was calculated by Equation (13):

$$F_r = \frac{2\pi n T_{stepper}}{S}, \quad (13)$$

The transmission efficiency n of the lead screw is generally 85–90%. Therefore, the thrust of the nut on the lead screw driven by the motor is 1601.4–1695.6 N.

When the motor is not driven, φ_2 in the unilateral underactuated mechanism is 120° and $\theta = 26^\circ$ as shown in Figure 9. Therefore, according to the requirements of the design scheme, a torsional spring was placed in the distal knuckle D to restrict the relative rotation of the two joints. According to the picking requirements and previous design experience [31], rods AB , BG , and L_{CF} were set as 50, 50, and 65 mm, respectively. The length of the bottom plate was set to 130 mm to avoid affecting the enveloping effect of the manipulator with a short-frame bottom plate. The length and width of the cutting blade were designed to be 80 and 50 mm, respectively, to ensure that the manipulator can cut at one time. The objective function was designed to optimize the length of rod CF and determine its parameters, as shown in Equation (14).

$$\begin{cases} F_2 l_2 > T_1 \\ F_2 = F_3 \cos \theta \end{cases}, \quad (14)$$

When the unilateral underactuated mechanism contacts broccoli, rod AD remains stationary, and the driving force overcomes the binding force of the torsional spring and continues to drive the swing rod DK to move. At this time, φ_2 is 102° , and the change of $\angle CDA$ at joint D is 18° . Therefore, the torsional spring torque T_1 is -1268.4 N·mm and the constraint condition is set as $30 \text{ N} \leq F_3 \leq 35 \text{ N}$. The following results were obtained according to the constraints of F_3 .

$$\begin{cases} F_3 = 35 \text{ N}, l_2 > 38.81 \text{ mm} \\ F_3 = 30 \text{ N}, l_2 > 45.28 \text{ mm} \end{cases}$$

Therefore, l_2 is rounded to 50 mm, and L_{DK} is 50 mm.

Additionally, the objective function was designed according to the design scheme and picking requirements, as shown in Equation (15), to optimize and determine the length of rod AD .

$$T_0 \geq 2F_{cy}l_1 + F_2l_2 + T_1, \quad (15)$$

Substituting the cutting force into the above equation and setting the constraint condition to $30 \text{ N} \leq F_3 \leq 35 \text{ N}$ obtained the following results:

$$\begin{cases} F_3 = 30 \text{ N}, l_1 \leq 46.44 \text{ mm} \\ F_3 = 35 \text{ N}, l_1 \leq 44.36 \text{ mm} \end{cases}$$

The height of the plants left after cutting was ensured to be 12–15 cm, and the structure was kept compact by setting l_1 to 45 mm and rods BC and AD to 90 mm.

Substituting $l_1 = 45 \text{ mm}$, $l_2 = 50 \text{ mm}$, $T_0 = 5357.13 \text{ N}\cdot\text{mm}$, and $T_1 = -1268.4 \text{ N}\cdot\text{mm}$ into Equation (12) yielded the following results:

$$\begin{cases} F_1 = 23.08 \text{ N} \\ F_2 = 32.57 \text{ N} \\ F_3 = 34.89 \text{ N} \end{cases}$$

In this result, the flower ball surface pressure F_1 is 23.08 N, whereas the pressure range in the previous paper is 25–30 N. Therefore, this result is less than the pressure range and

meets the requirement of low-loss picking. In addition, the cutting force F_3 in this result is 34.89 N, which conforms to the cutting force range of 30–35 N in the stem-cutting test and meets the requirements for picking.

Therefore, the parameters of each rod are shown in Table 2.

Table 2. Parameters of the connecting rods of the underactuated mechanism (unit: mm).

Symbol	L_{AB}	L_{BC}	L_{CD}	L_{AD}	L_{DK}	L_{BG}	L_{CF}
Parameter	50	90	50	90	50	60	65

3.5. Determination of Underactuated Mechanism Thrust

F_1 and F_2 in Equation (11) can be obtained by Equation (16):

$$T_0 = F_1 l_1 + (d \cos \theta_3 + l_2) F_2, \tag{16}$$

The following can be obtained from Equation (8):

$$F_{T_0} = \frac{T_0}{a \cos \alpha \sin(\frac{\pi}{2} - \alpha)}, \tag{17}$$

Substituting $l_1 = 45 \text{ mm}$, $l_2 = 50 \text{ mm}$, $d = 90 \text{ mm}$, $\theta = 21^\circ$, $\theta_3 = 18^\circ$, $\alpha = 55^\circ$, $25 \text{ N} \leq F_1 \leq 30 \text{ N}$, and $25 \text{ N} \leq F_2 \leq 30 \text{ N}$ into Equations (16) and (17) resulted in:

$$\begin{cases} F_1 = 25 \text{ N}, F_2 = 28.01 \text{ N}, F_{T_0} = 299.28 \text{ N} \\ F_1 = 25 \text{ N}, F_2 = 32.68 \text{ N}, F_{T_0} = 337.77 \text{ N} \\ F_1 = 30 \text{ N}, F_2 = 28.01 \text{ N}, F_{T_0} = 312.95 \text{ N} \\ F_1 = 30 \text{ N}, F_2 = 32.68 \text{ N}, F_{T_0} = 351.44 \text{ N} \end{cases}$$

The manipulator has a symmetrical structure of the manipulator; therefore, thrust F_T was calculated as shown in Equation (18):

$$F_T = 2F_{T_0}, \tag{18}$$

The required thrust F_T range of the manipulator is 598.66–702.88 N. According to the result, the thrust of the motor drive nut is greater than that required by the underactuated mechanism:

$$F_T > F_T = 2F_{T_0}. \tag{19}$$

Therefore, the thrust of the stepper motor meets the requirements of picking and the requirements of the scheme design of the underactuated mechanism.

4. Broccoli-Picking Test

4.1. Simulation Analysis of Manipulator Motion

Aluminum alloy material, 302 steel, and S304 material were imported into the manipulator in Adams software, and constraints were added to further verify the rationality of the design of the manipulator. The manipulator motion simulation was completed at a driving force of 2000 N and a moving plate speed of 5.5 mm/s. Marker points were added to the contact position between the middle of the clamping guard plates and the contact position between the cutting blades and the stem of the mechanical hand to measure the contact force of the two positions after the simulation (Figure 10), thus verifying the reasonable design of the manipulator.

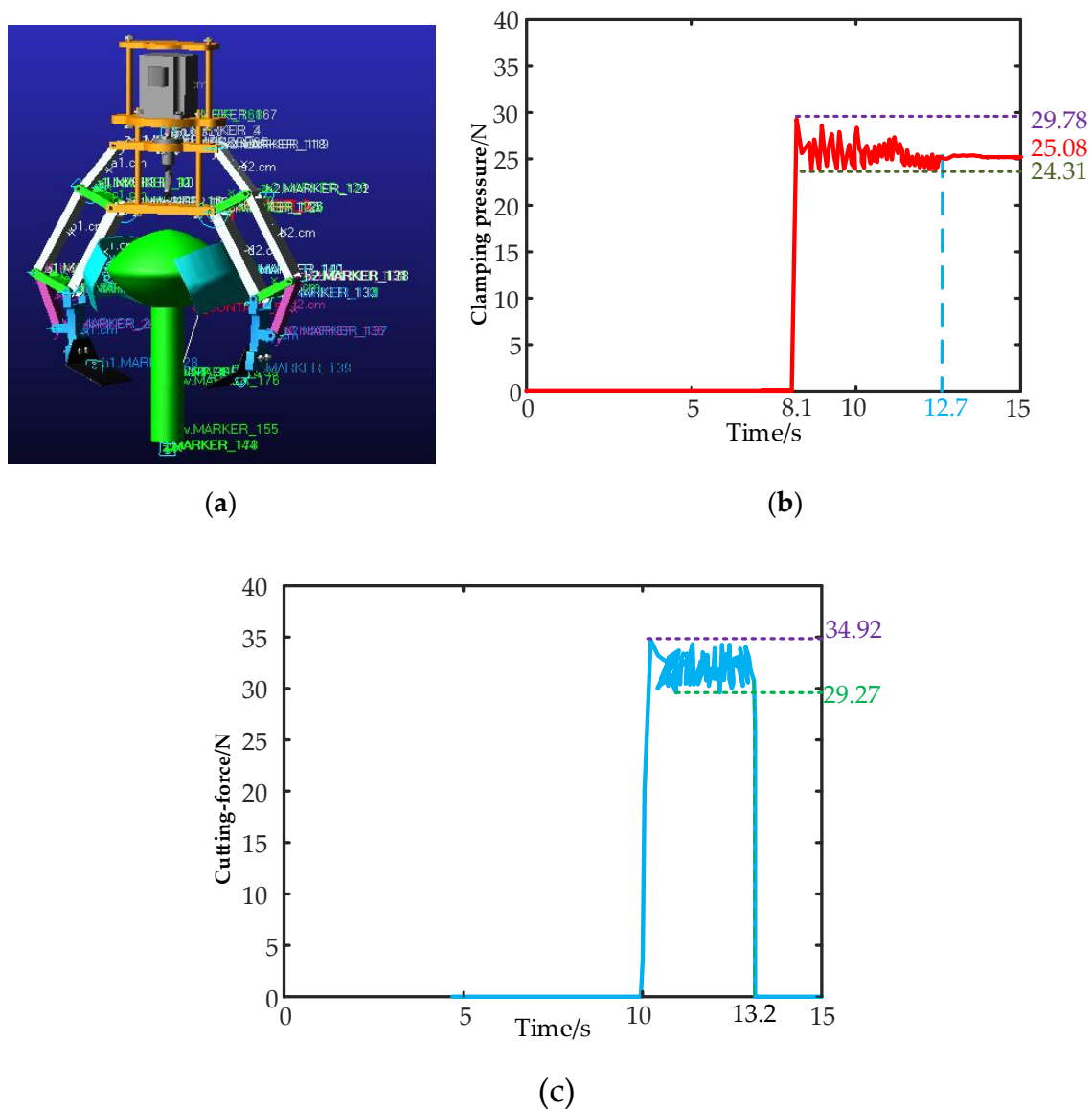


Figure 10. Manipulator motion simulation: (a) Manipulator motion simulation; (b) Clamping pressure curve; (c) Cutting force curve.

In Figure 10b, the red curve represented the pressure on the guard plates when the manipulator was clamping the flower ball, and the blue line represented the pressure stabilization time point. At 12.7 s, the clamping pressure tended to stabilize at 25.08 N, while purple represented the maximum pressure of 29.78 N and green represented the minimum pressure of 24.31 N. In Figure 10c, the blue curve represented the pressure on the blade when the manipulator was cutting the stem. When the cutting was finished at 13.2 s, the cutting force was 0 N. Purple represented the maximum cutting force of 34.92 N and green represented the minimum cutting force of 29.27 N. Therefore, it can be concluded from Figure 10b,c that the flower ball surface pressure and stem cutting force in the simulation test were basically consistent with the forces tested in the actual test above.

4.2. Broccoli-Picking Test Stand Set Up

According to the requirements of planting and picking, the feasibility of the picking manipulator was verified by setting up a picking test stand. Set up a picking test stand in the laboratory environment, as shown in Figure 11. The length, width, and height of the test stand support frame are 108, 100, and 120 cm, respectively, as shown in Figure 11(1). The control cabinet was placed on the upper layer of the support frame, as shown in Figure 11(2).

Figure 11(3) shows that the Siasun GCR5-910 robot arm with six degrees of freedom was hung upside down in the middle of the support frame of the test stand. The manipulator was connected to the end flange of the robot arm, as shown in Figure 11(4). A telepad with a length, width, and height of 120, 30, and 20 cm, respectively, was placed in the middle of the support frame of the test stand to simulate ridge planting conditions. Broccoli plant fixers were installed at 40 cm intervals on the telepad, as shown in Figure 11(5). Baskets with a height of 20 cm and a diameter of 30 cm were placed at the four corners horizontally from the middle point of the support frame, as shown in Figure 11(6).

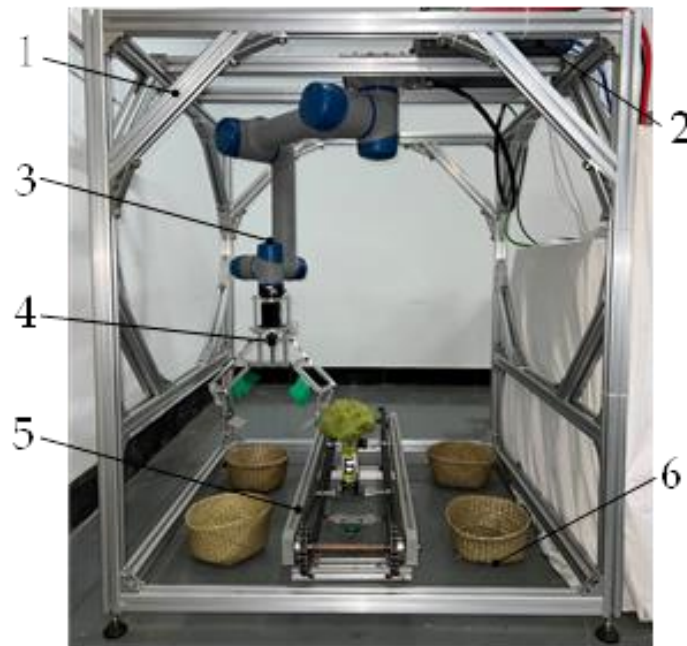


Figure 11. Broccoli-picking test stand: (1) test stand support frame; (2) control cabinet; (3) robot arm; (4) manipulator; (5) telepad; (6) baskets.

4.3. Establishment of Broccoli-Picking Control System

The control system of the picking test stand is composed of a manipulator with six degrees of freedom, a control cabinet, an underactuated manipulator, a stepper motor, and a stepper motor controller. The schematic diagram of the control system of the picking test stand is shown in Figure 12.

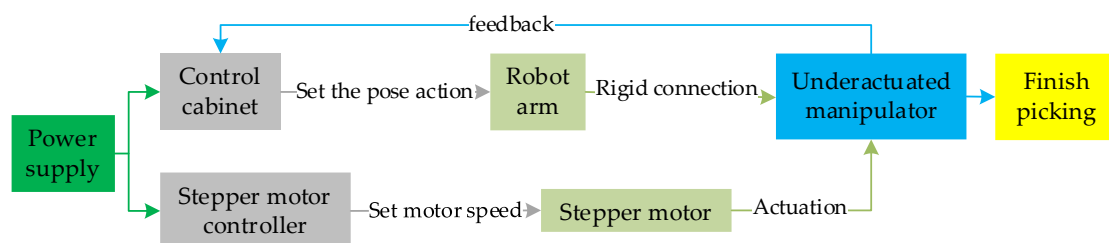


Figure 12. Diagram of the broccoli-picking test stand system.

The motion trajectory of the mechanical arm was planned in advance, and the motion path and posture of the robot arm were determined directly through the demonstrator to facilitate the determination of the position of the broccoli. In this way, the clamping and unloading time of the manipulator was set to 2.5 s, and the speed of the stepper motor was adjusted to 60 r/min. The picking test was carried out in the picking test environment without interference.

4.4. The Picking Test of Testbed

First, the power supply is turned on. After the robot arm is fully started, the manipulator is driven to the top of the broccoli plant through the control panel. The underactuated mechanism gradually approaches the plant under the motor drive (Figure 13a). The manipulator holds the guard plates and cutting blade in contact with the plant (Figure 13b). Broccoli is cut under the motor drive (Figure 13c) and reaches the top of the harvest basket under the traction of the robot arm. The manipulator opens under the drive of the motor, and the broccoli falls into the harvest baskets (Figure 13d). The process is shown in Figure 13.

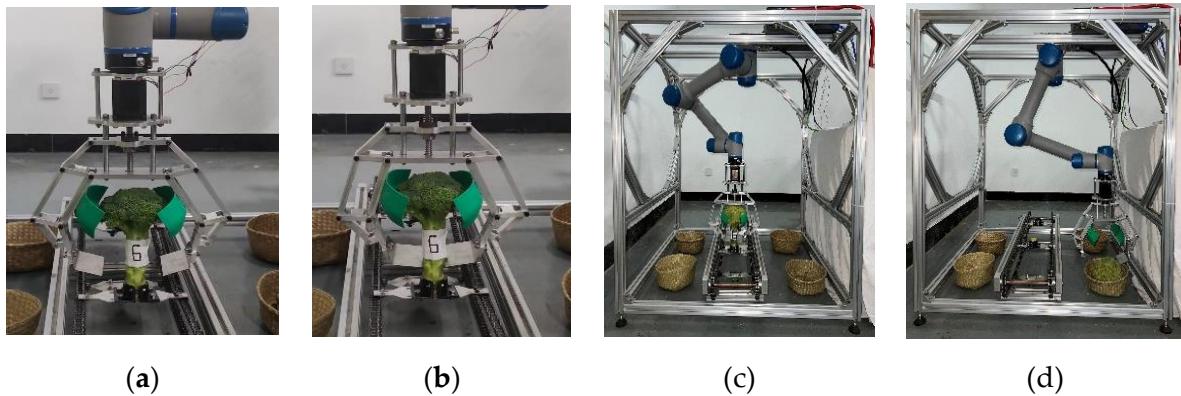


Figure 13. Experimental picking process of broccoli: (a) The manipulator moves closer to the broccoli; (b) The manipulator contacts the broccoli; (c) Clamping and cutting; (d) Broccoli is released into the harvest basket.

5. Experiment and Analysis of Picking

5.1. Material and Method

The picking experiment was carried out on 6 November 2022. A simulated picking test was conducted under an experimental environment to verify the success rate, non-destructive rate, and picking efficiency of the mechanism. In the early stage of the experiment, the flower balls of 100 broccolis were divided into five groups with 20 broccolis each according to their diameter: 135–145, 145–155, 155–165, 165–175, and 175–185 mm. When the broccolis were brought back, their leaves had been removed; therefore, the broccolis in the experiment had no leaves; The manipulator was opened to a maximum size of 21 cm by the stepper motor drive. The broccoli was then attached to the telepad, as shown in Figure 14. Then, the test was carried out in the way described above, and these test data were recorded.

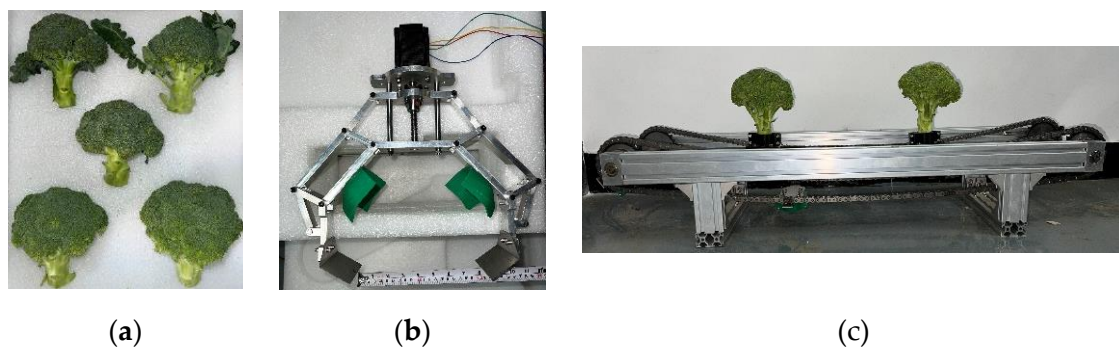


Figure 14. Test material: (a) Broccoli of different diameters; (b) Initial state of the manipulator; (c) Broccoli-picking location.

5.2. Analysis of Picking Results

The criteria for successful harvest were divided into three conditions: planting retention height, flower ball extrusion state, and stem incision state (Figure 15).

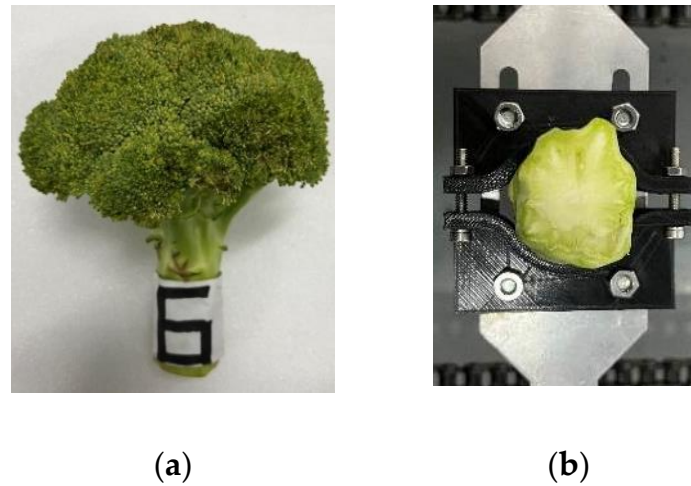


Figure 15. Successful picking factors: (a) Clamping damage was low, and plant height was greater than 12 cm; (b) The incision surface was flat and non-adhesive.

Ten broccoli plants were selected from each of the five groups to determine the success rate of picking. The robot arm ran at 2.8 m/s, and the stepper motor ran at 60 r/min. As shown in Table 3, the success rate of broccoli picking can reach 84% on average.

Table 3. The success rate of picking.

Group	Flower Ball Diameter (mm)	Total Number of Picks	Number of Successful Picks	Number of Picking Failures	Picking Success Rate (%)	Number of Broccolis with Harvesting Heights Higher than 12 cm
1	135–145	10	8	2	80	9
2	145–155	10	9	1	90	10
3	155–165	10	9	1	90	9
4	165–175	10	8	2	80	10
5	175–185	10	8	2	80	8
	Total	50	42	8	84	46

Afterward, 10 broccoli plants were sampled from each of the five groups. The average harvesting time of a single broccoli plant was calculated under the five different moving speeds of the robot arm. The results are shown in Table 4.

Table 4. Average harvesting time under different movement speeds.

Motion Speed of the Arm (m/s)	Average Time for the Arm to Reach the Broccoli (s)	Average Time for the Arm to Finish Picking (s)	Average Time to Release to Harvest Basket (s)	Total Time (s)	Number of Broccoli with Harvesting Height Higher than 12 cm
2.2	2.86	2.02	10.23	15.11	10
2.5	2.57	2.02	9.32	13.91	9
2.8	2.33	2.02	8.55	12.9	8
3.1	2.31	2.02	7.18	11.51	10
3.4	2.27	2.02	7.08	11.37	9

When the speed of the robot arm exceeded 3.4 m/s, the picking test bench shook violently under the action of inertia. Therefore, the fastest single flower ball harvesting speed was 11.37 s in the laboratory environment when the arm speed was 3.4 m/s, and the stepper motor speed was 60 r/min.

Mechanical damage characteristics of fruits and vegetables include static pressure, vibration, and impact damage [32]. However, the manipulator used in this paper exerts pressure on flower balls during the picking process. According to the simulation test

and damage observation of 100 post-harvest flower balls, the pressure generated by the manipulator does not damage the flower ball surface. Therefore, the non-destructive rate of picking 100 broccoli flower balls was 100%.

5.3. Manipulator Characteristic Evaluation

In this paper, a symmetrical clamping and cutting style broccoli picking manipulator is designed based on the underactuated principle, which has the following characteristics.

(1) The manipulator has a simple and compact structure and simple control system, and stable configuration when picking broccoli.

(2) In the laboratory environment, the success rate of picking broccoli with the six-degree-of-freedom robot arm equipped with the manipulator was 84%, and the non-destructive rate was 100%.

(3) In the closed state, the maximum strength of the manipulator is 28 cm, the widest part is 21 cm, and the overall mass is 3.86 kg. Therefore, the size of the manipulator can be further reduced in the future to make the structure more flexible and lightweight processing. Thus applicable to other cruciferous ball-type vegetables.

6. Conclusions

(1) According to the physical characteristics of broccoli, a symmetrical double-finger underactuated manipulator was designed for picking operation by means of clamping and cutting.

(2) According to the surface pressure and stem-cutting force test of the broccoli flower ball and the analysis of kinematics and static mechanics of the underactuated manipulator, each connecting rod of the underactuated mechanism was determined to be 50 cm, 90 cm, and 50 cm, 90 cm, 50 cm, 60 cm, 65 cm, and the driving force of the manipulator was 598.66 N–702.88 N. The manipulator has the ability to pick broccoli with a diameter of 135 mm–185 mm. The reliability of the manipulator was verified by the simulation analysis of the manipulator motion.

(3) According to the requirements of broccoli planting and picking, picking test in a broccoli-picking test stand through the laboratory environment with 100 broccolis proved that the manipulator had a picking success rate of 84% and a lossless rate of 100% when the speed of the arm was 3.4 m/s, and the speed of the stepper motor was 60 r/min. The fastest single harvest time of the test stand was 11.37 s.

Author Contributions: Original draft, investigation, resources, validation, review and editing, H.X., C.N. and Y.C.; Supervision, review, and editing, funding acquisition, G.Y.; Methodology, data curation, software, visualization, conceptualization, C.N. and H.X.; Project administration, G.Y. and X.Z.; Formal analysis, Y.W. and H.X. All authors have read and agreed to the published version of the manuscript.

Funding: This research was funded by the Key Research and Development Project of the Science and Technology Department of Zhejiang Province, China, grant number 2021C02021; National key research and development program, China, (No. 2022YFD2001800).

Institutional Review Board Statement: Not applicable.

Informed Consent Statement: Not applicable.

Data Availability Statement: Not applicable.

Acknowledgments: Key Research and Development Project of the Science and Technology Department of Zhejiang Province, China, (No. 2021C02021); National key research and development program, China, (No. 2022YFD2001800).

Conflicts of Interest: The authors declare no conflict of interest.

References

1. Aloo, S.O.; Ofosu, F.K.; Kilonzi, S.M.; Shabbir, U.; Oh, D.H. Edible plant sprouts: Health benefits, trends, and opportunities for novel exploration. *Nutrients* **2021**, *13*, 2882. [[CrossRef](#)] [[PubMed](#)]
2. Li, Z.S.; Liu, Y.M.; Fang, Z.Y.; Yang, L.M.; Zhuang, M.; Zhang, Y.Y.; Lv, H.H.; Wang, Y. Development status, existing problems, and coping strategies of the Chinese broccoli industry. *China Veg.* **2019**, *4*, 1–5. (In Chinese) [[CrossRef](#)]
3. Vrochidou, E.; Tsakalidou, V.N.; Kalathas, I.; Gkrimpizis, T.; Pachidis, T.; Kaburlasos, V.G. An Overview of End Effectors in Agricultural Robotic Harvesting Systems. *Agriculture* **2022**, *12*, 1240. [[CrossRef](#)]
4. Biswas, N.; Aslekar, A. Improving Agricultural Productivity: Use of Automation and Robotics. In Proceedings of the 2022 International Conference on Decision Aid Sciences and Applications, Chiangrai, Thailand, 23–25 March 2022. [[CrossRef](#)]
5. Zhang, B.; Xie, Y.; Zhou, J.; Wang, K.; Zhang, Z. State-of-the-Art robotic grippers, grasping and control strategies, as well as their applications in agricultural robots: A review. *Comput. Electron. Agric.* **2020**, *177*, 105694. [[CrossRef](#)]
6. Wang, Z.; Xun, Y.; Wang, Y.; Yang, Q. Review of smart robots for fruit and vegetable picking in agriculture. *Int. J. Agric. Biol. Eng.* **2022**, *15*, 33–54. [[CrossRef](#)]
7. Mochiyama, H.; Gunji, M.; Niiyama, R. Ostrich-Inspired Soft Robotics: A Flexible Bipedal Manipulator for Aggressive Physical Interaction. *J. Robot. Mechatron.* **2022**, *34*, 212–218. [[CrossRef](#)]
8. Hota, R.K.; Kumar, C.S. Effect of design parameters on strong and immobilizing grasps with an underactuated robotic hand. *Robotica* **2022**, *40*, 3769–3785. [[CrossRef](#)]
9. Birrell, S.; Hughes, J.; Cai, J.Y.; Iida, F. A field-tested robotic harvesting system for iceberg lettuce. *J. Field Robot.* **2020**, *37*, 225–245. [[CrossRef](#)]
10. He, T.; Aslam, S.; Tong, Z.; Seo, J. Scooping manipulation via motion control with a two-fingered gripper and its application to bin picking. *IEEE Robot. Autom. Lett.* **2021**, *6*, 6394–6401. [[CrossRef](#)]
11. Gao, G.; Chapman, J.; Matsunaga, S.; Mariyama, T.; MacDonald, B.; Liarokapis, M. A Dexterous, Reconfigurable, Adaptive Robot Hand Combining Anthro-morphic and Interdigitated Configurations. In Proceedings of the 2021 IEEE/RSJ International Conference on Intelligent Robots and Systems, Prague, Czech Republic, 27 September–1 October 2021. [[CrossRef](#)]
12. Williams, H.A.; Jones, M.H.; Nejati, M.; Seabright, M.J.; Bell, J.; Penhall, N.D.; Barnett, J.J.; Duke, M.D.; Scarfe, A.J.; Ahn, H.S.; et al. Robotic kiwifruit harvesting using machine vision, convolutional neural networks, and robotic arms. *Biosyst. Eng.* **2019**, *181*, 140–156. [[CrossRef](#)]
13. Kinugawa, J.; Suzuki, H.; Terayama, J.; Kosuge, K. Underactuated robotic hand for a fully automatic dishwasher based on grasp stability analysis. *Adv. Robot.* **2022**, *36*, 167–181. [[CrossRef](#)]
14. Xiong, Y.; Ge, Y.; Grimstad, L.; From, P.J. An autonomous strawberry-harvesting robot: Design, development, integration, and field evaluation. *J. Field Robot.* **2020**, *37*, 202–224. [[CrossRef](#)]
15. Arad, B.; Balendonck, J.; Barth, R.; Ben-Shahar, O.; Edan, Y.; Hellström, T.; Hemming, J.; Kurtser, P.; Ringdahl, O.; Tielen, T.; et al. Development of a sweet pepper harvesting robot. *J. Field Robot.* **2020**, *37*, 1027–1039. [[CrossRef](#)]
16. Zhao, Y.W.; Geng, D.X.; Liu, X.M.; Sun, G.D. Kinematics Analysis and Experiment on Pneumatic Flexible Fruit and Vegetable Picking Manipulator. *Trans. Chin. Soc. Agric. Mach.* **2019**, *50*, 31–42. (In Chinese) [[CrossRef](#)]
17. Jia, J.M.; Ye, Y.Z.; Cheng, P.L.; Zhu, Y.P.; Fu, X.P.; Chen, J.N. Design and Experimental Optimization of Hand-held Manipulator for Picking Famous Tea Shoot. *Trans. Chin. Soc. Agric. Mach.* **2022**, *53*, 86–92. (In Chinese) [[CrossRef](#)]
18. Cui, Y.J.; Ma, L.; He, Z.; Zhu, Y.T.; Wang, Y.C.; Li, K. Design and Experiment of Dual Manipulators Parallel Harvesting. *Trans. Chin. Soc. Agric. Mach.* **2022**, *53*, 132–143. (In Chinese) [[CrossRef](#)]
19. Yin, J.J.; Chen, Y.H.; He, K.; Liu, J.Z. Design and Experiment of Grape-picking Device with Grasping and Rotary-cut Type of Underactuated Double Fingered Hand. *Trans. Chin. Soc. Agric. Mach.* **2017**, *48*, 12–20. (In Chinese) [[CrossRef](#)]
20. Ma, T.; Yang, D.; Zhao, H.W.; Li, T.; Ai, N. Grasp Analysis and Optimal Design of a New Underactuated Manipulator. *Robot* **2020**, *42*, 354–364. (In Chinese) [[CrossRef](#)]
21. Chen, W.; Xiong, C.; Chen, W.; Yue, S. Mechanical adaptability analysis of underactuated mechanisms. *Robot. Comput. -Integr. Manuf.* **2018**, *49*, 436–447. [[CrossRef](#)]
22. Lei, X.P.; Tang, S.F.; Liang, W.; Guo, Z.R. Optimization Design and Grasping Stability Analysis of Under-actuated Multi-finger Manipulator. *J. Mech. Transm.* **2020**, *44*, 53–58. (In Chinese) [[CrossRef](#)]
23. Guo, H.S.; Ma, R.; Zhang, Y.X.; Li, Z.Y. Design and Simulation Analysis of Ya Shaped Underactuated Korla Fragrant Pear Picking Manipulator. *J. Agric. Mech. Res.* **2023**, *45*, 110–117. (In Chinese) [[CrossRef](#)]
24. El Didamony, M.I.; El Shal, A.M. Fabrication and evaluation of a cabbage harvester prototype. *Agriculture* **2020**, *10*, 631. [[CrossRef](#)]
25. Blok, P.M.; Van, E.F.K.; Tielen, A.P.M.; Van Henten, E.J.; Kootstra, G. The effect of data augmentation and network simplification on the image-based detection of broccoli heads with Mask R-CNN. *J. Field Robot.* **2021**, *38*, 85–104. [[CrossRef](#)]
26. Calzado, J.; Lindsay, A.; Chen, C.; Samuels, G.; Olszewska, J.I. SAMI: Interactive, Multi-sense Robot Architecture. In Proceedings of the 2018 IEEE 22nd International Conference on Intelligent Engineering Systems, Las Palmas de Gran Canaria, Spain, 21–23 June 2018. [[CrossRef](#)]
27. Wang, Y.; Wang, Wen, Z.J.; Lian, Y.; Hu, S.; Li, X.J.; Shao, X.G. Broccoli Harvesting Machine. China Patent 201821455355.X, 2 April 2019. (In Chinese)
28. Du, J.C.; Yu, H.M.; Zhang, J.W.; Chen, Y.T.; Chen, K.J. Design on Broccoli Harvesting Suspension Bucket Based on ANSYS. *Agric. Eng.* **2019**, *9*, 102–107. (In Chinese) [[CrossRef](#)]

29. Zhang, X.M.; Chen, X.A.; Hou, X.N.; Liu, S.Y.; Xie, P.F. A Selective Broccoli Harvester. China Patent 202211324085 X, 31 January 2023. (In Chinese)
30. Zhao, Y.F.; Han, F.F.; Tang, Z.; Chen, S.R.; Ding, H.T. A Kind of Harvester for Precise Cutting of Broccoli. China Patent 202210599247.4, 16 August 2022. (In Chinese)
31. Niu, C.Y. Design and Experiment of Broccoli Harvesting Manipulator. Master's Thesis, Zhejiang Sci-Tech University, Hang Zhou, China, 1 April 2022. (In Chinese)
32. Zaicovski, C.B.; Pegoraro, C.; Ferrarezze, J.P.; Cero, J.D.; Lund, D.G.; Rombaldi, C.V. Effects of mechanical injury, temperature decreasing, and 1-MCP on the post-harvest metabolism of Legacy broccoli. *Food Sci. Technol.* **2008**, *28*, 840–845. [[CrossRef](#)]

Disclaimer/Publisher's Note: The statements, opinions and data contained in all publications are solely those of the individual author(s) and contributor(s) and not of MDPI and/or the editor(s). MDPI and/or the editor(s) disclaim responsibility for any injury to people or property resulting from any ideas, methods, instructions or products referred to in the content.